Star formation in clusters: early sub-clustering in the Serpens core

Leonardo Testi[1,2,5], Anneila I. Sargent[2], Luca Olmi[3] and Joseph S. Onello[4]

ABSTRACT

We present high resolution interferometric and single dish observations of molecular gas in the Serpens cluster-forming core. Star formation does not appear to be homogeneous throughout the core, but is localised in spatially- and kinematically-separated sub-clusters. The stellar (or proto-stellar) density in each of the sub-clusters is much higher than the mean for the entire Serpens cluster. This is the first observational evidence for the hierarchical fragmentation of proto-cluster cores suggested by cluster formation models.

Subject headings: ISM: clouds – ISM: radio continuum – stars: formation

1. Introduction

It is generally accepted that most stars are born in clusters (cf. Clarke et al. 2000). The way in which clusters form and evolve is therefore likely to influence the distribution of masses for stars in the field, the initial mass function, IMF (Salpeter 1955; Scalo 1986). In very young, embedded clusters the distribution of stellar masses is often similar to the IMF (Palla & Stahler 1999; Meyer et al. 2000), and the mass spectra of prestellar and protostellar condensations in the Serpens and ρ–Ophiuchi cluster-forming cores are also consistent with the IMF (Testi & Sargent 1998, hereafter TS98; Motte et al. 1998).

It has been suggested that within stellar clusters star formation occurs preferentially in sub-clusters where the stellar density is much enhanced (Clarke et al. 2000). This

[1]Osservatorio Astrofisico di Arcetri, Largo E. Fermi 5, I-50125 Firenze, Italy

[2]Division of Physics, Mathematics and Astronomy, California Institute of Technology, MS 105-24, Pasadena, CA 91125, USA

[3]LMT Project and FCRAO, University of Massachusetts, 630 L.G.R.C., Amherst, MA 01003, USA

[4]Department of Physics, State University of New York, Cortland, NY 13045, USA

[5]ltesti@arcetri.astro.it

has important implications for cluster evolution. For example, more massive stars could be produced by coalescence (Stahler et al. 2000). To date, there is little evidence for sub-clustering in the Orion Nebula Cluster (Bate et al. 1998) or in the smaller clusters around intermediate mass pre-main sequence stars (Testi et al. 1999). However, models advocate sub-clusters with a much higher stellar density at the time of formation (Bonnell et al. 1998). It is therefore important to establish if sub-clustering is present in the very youngest clusters. The mean stellar densities and the stellar to gas mass ratio in such sub-clusters can provide critical observational constraints on coalescence, competitive accretion and binary evolution models (Bonnell et al. 1997; 1998; Kroupa 1999).

The Serpens molecular cloud, at ~ 310 pc (de Lara et al. 1991), is one of the most active nearby cluster-forming cores. Inside the 500–1500 $M_\odot$, ~ 0.6 pc diameter cloud of molecular gas (White et al. 1995) is a young protocluster comprising about one hundred embedded young stellar objects (YSOs), protostars and prestellar clumps (Strom et al. 1976; Eiroa & Casali 1992; Giovannetti et al. 1998; Kaas 1999; Casali et al. 1993; Hurt & Barsony 1993; TS98). Numerous jets and molecular outflows have also been detected (Rodríguez et al. 1989; White et al 1995; Eiroa et al. 1997; Herbst et al. 1997; Wolf-Chase et al. 1998; Davis et al. 1999; Hodapp 1999; Hogerheijde et al. 1999). The total estimated mass of the YSOs, protostars, and prestellar clumps is in the range 40–80 $M_\odot$ (Giovannetti et al. 1998; TS98), implying an overall star formation efficiency of 2–5%, similar to most nearby molecular clouds. The proto-cluster radius, ~ 0.2 pc, and mean stellar density, $\sim 400\text{-}800$ stars/pc^3, are typical of very young embedded clusters (Testi et al. 1999), making this an ideal laboratory for studying early cluster formation processes. Here, we present wide field, high resolution, aperture synthesis and single dish millimeter-wave molecular line observations of the Serpens core which support the concept of at-birth sub-clustering.

2. Observations and results

Owens Valley Radio Observatory (OVRO) millimeter wave array mosaic observations of the $5.5' \times 5.5'$ inner region of the Serpens molecular core in the CS(2–1) transition at 97.98 GHz were obtained at the same time as the 3 mm continuum data described by TS98. Details of the observations, data reduction, and mosaic construction are described elsewhere (TS98; Testi & Sargent 2000). Spectral resolution was 0.4 km/s over a 24 km/s bandwidth centered at $V_{\rm LSR} = 8$ km/s. The synthesized beam is $5''.5 \times 4''.3$ (FWHM), and the noise level in each channel of the final cleaned mosaic cube is ~ 140 mJy/beam. During spring/fall 1998, additional observations of SMM4, S68N and the CS6, CS7 and CS8 features identified in Figure 1a were acquired (Testi & Sargent 2000). The digital correlator

was configured so that the $N_2H^+(1\text{–}0)$ transition at 93.2 GHz and the $CH_3OH(2_{-1}\text{–}1_{-1})E2$ and $(2_0\text{–}1_0)A^+$ transitions at 96.7 GHz were detected simultaneously in the lower and upper sidebands respectively. Spectral resolution was 0.4 km/s over a 25 km/s band. Calibration was carried out as in TS98. The datasets were imaged using the AIPS IMAGR task.

A $10' \times 10'$ region of the Serpens cloud core, centered on $\alpha = 18^h27^m20^s$, $\delta = 1°12'30''$ (B1950.0), was also mapped in the $N_2H^+(1\text{–}0)$ line in March and October 1999, using the 13.7-m telescope of the Five College Radio Astronomy Observatory[6] (FCRAO) and the SEQUOIA focal plane array. For the one beam sampled maps, the half power beam width (HPBW) was $\sim 52''$. Low noise InP MMIC-based amplifiers resulted in mean receiver temperature of 70 K (SSB), and system temperatures of 160–250 K. The spectrometer was an autocorrelator with 24 kHz (0.077 km/s) spectral resolution and 20 MHz bandwidth. Typical integration times were 5 to 15 minutes in frequency switching mode, with a throw of 8 MHz. The main beam efficiency, to convert the antenna temperature to brightness temperature, η_{mb}, is 0.51, and the final rms was ~ 0.05 K (T_{mb}).

2.1. OVRO maps

In Figures 1a and 1b we show the CS(2–1) integrated intensity mosaic overlaid on our 3mm continuum map (TS98) and the CS(2–1) mean velocity mosaic, respectively. In Fig. 1a some of the brightest CS(2–1) features are labelled to simplify discussion; the location of the NIR cluster surrounding SVS-2 and SVS-20 (Strom et al. 1976) is also indicated. In Fig. 1b, the orientations of the jets emanating from SMM1, SMM3, SMM4, and A3, as well as the NIR reflection nebula associated with SMM5 are marked.

At most, 20% of the flux detected in single dish maps of the optically thick and extended CS(2–1) emission (cf. McMullin et al. 1994) is recovered. There is therefore little point in comparing the CS and the optically thin 3 mm emission (TS98). However, the molecular line observations provide information about the outflows emanating from the various millimeter sources; the abundance of CS can increase by a factor of almost 100 in outflows (Bachiller & Pérez Gutiérrez 1997), and most of the clumps in Figure 1a are likely to be compact enhancements in shocked regions. In most cases the CS linewidths are relatively broad, $\geq$2–3 km/s, and mean velocities differ by 3-4 km/s from the systemic velocity of the Serpens core (Figure 1b). Strong and broad CH_3OH emission, typical of shocked material, was also seen in our followup observations (Figure 2), and coincides with

the CS features. By contrast N_2H^+ emission is spatially coincident with the continuum sources, as expected for a tracer of cores and envelopes.

2.2. FCRAO N_2H^+ map

Figure 3 shows the FCRAO/SEQUOIA large scale channel maps of the $N_2H^+(1_{01}–0_{12})$ isolated hyperfine component. Four cores, labelled A, B, C, and D in order of increasing V_{LSR}, and an extended, lower surface brightness "spur" can be identified. The spur stretches from the NW (C, D) to SE (A, B) cores and continues beyond these. Cores A and B are spatially associated with the SMM3/SMM4 region, while C and D encompass the SMM1/S68N region. Spectra at the emission peaks in A, B, C, and D are also presented in Fig. 3. These positions are given in Table 1 as offsets from $\alpha = 18^h27^m20^s$, $\delta = 1°12'30''$. Also listed are the V_{LSR}, line width, ΔV, and virial mass, M_{vir}, for each core. The fraction of the total N_2H^+ flux observed with the array is f_{OVRO}; M_d is the total mass of 3 mm continuum cores within each gaseous core (TS98), and $M_\star$ is the total mass of YSOs, derived assuming a mean stellar mass of 0.3 $M_\odot$ (Giovannetti et al. 1998; Kaas 1999). The FCRAO and OVRO values of ΔV and V_{LSR} are consistent, suggesting that the array is detecting a fraction of the emission from extended envelopes, rather than the compact cores found by TS98.

2.3. Identification of outflow sources

The powering sources of the CS outflows were identified from published optical, infrared and millimeter observations, and are represented by open diamonds in Figure 1. Features CS3 and CS4 as well as CH_3OH emission (Fig. 2) suggest a compact outflow at p.a.~140°, centered on the S68N continuum source (cf. Wolf-Chase et al. 1998). CS2 could either be an extension of the S68N flow or the counterflow of the H_2 jet from mm source A3 (Hodapp 1999; TS98). Based on its alignment with an H_2 jet (Hodapp 1999) and the locations of HH460 and a CO(2–1) bullet (Davis et al. 1999), we associate CS1 with an outflow from SMM1. CS6, CS7, and CS8 probably mark the interaction of the counterflow from SMM1 with the B molecular core. All these outflows are oriented along p.a.~140°. A double-peaked CS component reported by Williams & Myers (1999) at the position of CS1 was not detected; it is probably extended and resolved out in our observations.

In the south-east, CS9 and CS10 are oriented like CH_3OH (Fig. 2) and H_2 knots near SMM4 (Eiroa et al. 1997) along p.a.~180°, and are probably part of an outflow centered

on that source (c.f. Hogerheijde et al. 1999). Likewise CS12 is elongated along p.a.~170° as are a chain of H_2 knots associated with SMM3 (Herbst et al. 1997). Davis et al. (1999) noted that two Herbig-Haro objects and SMM3 are aligned along a position angle which is almost orthogonal to the chain of H_2 knots. However, the kinematic properties of the knots suggest no physical connection with the HH objects.

3. Discussion

Our new interferometer and single-dish maps of the Serpens core indicate sub-clustering at an early epoch of cluster formation. Three separate properties argue for sub-clustering, spatial segregation, outflow orientations, and circumcluster gas kinematics. Approximately one third of the near infrared cluster members are concentrated in a ~0.1 pc radius region surrounding SVS-2 and SVS-20 (Giovannetti et al. 1998; Kaas 1999), while the millimeter and sub-millimeter sources are largely concentrated in the SE (A, B) and NW (C, D) fragments (TS98; Davis et al. 1999). The orientations of the outflows observed in the SE and NW are quite different. In the NW, all three flows are oriented along p.a.~140°, as is the near infrared reflection nebula centered on SMM5 (Kaas 1999; see also Figure 1b). In the SE, the two outflows are aligned approximately north-south, with mean p.a.~175°. In Figure 3, the NW and SE sub-clusters are embedded in discrete $N_2H^+(1-0)$ clumps, separated in velocity by ~1 km/s (Table 1). Each clump comprises two cores: peak velocities of cores A and B differ by only 0.5 km/s ($\sim 1/2\ \Delta V$), C and D by 0.1 km/s ($\sim 1/10\ \Delta V$). Thus the spatially distinct clumps are also kinematically separated, while there is reasonable internal velocity coherence.

It appears that the Serpens core encompasses at least three sub-structures – the NW and SE sub-clusters and the NIR cluster. Star formation is currently occurring simultaneously in the NW and SE sub-clusters, both of which contain roughly equal fractions of prestellar, protostellar and infrared sources. The NIR cluster is probably more evolved but we see no evidence of the progressive pattern of star formation proposed by Casali et al. (1993). The kinematics and outflow orientations indicate that each subcluster originated in a separate fragment of the cloud which subsequently fragmented into the smaller cores seen in the $N_2H^+(1-0)$ maps. Within these are the 3 mm continuum cores that are likely progenitors of single stellar systems (TS98). Taken together these observations are consistent with either the hierarchical fragmentation picture advocated by Elmegreen (1997; 1999) or the spontaneous fragmentation suggested by Myers (1998) for the formation of stellar clusters, and provide the first observational support for hierarchical fragmentation within a cluster-forming core. We note that while the mean stellar/protostellar density of

the entire Serpens core is $\sim$400-800 stars/pc^3, most of the proto-cluster members are within the three subclusters where densities reach 2000-4000 stars/pc^3. It is very likely that, within a few million years, the cluster will evolve to a size and mean density very similar to those of embedded clusters around intermediate mass stars.

REFERENCES

Bachiller, R., & Pérez Gutiérrez, M. 1997, ApJ, 487, L93

Bate, M.R., Clarke, C.J., & McCaughrean, M. 1998, MNRAS, 297, 1163

Bonnell, I.A., Bate, M.R., Clarke, C.J., Pringle, J.E. 1997, MNRAS, 285, 201

Bonnell, I.A., Bate, M.R., & Zinnecker, H. 1998, MNRAS, 298, 93

Casali, M. M., Eiroa, C., & Duncan, W. D. 1993, A&A, 275, 195

Caselli, P., Myers, P.C., & Thaddeus, P. 1995, ApJ, 455, L77

Clarke, C.J., Bonnell, I.A., & Hillenbrand, L.A. 2000, in Protostars and Planets IV, eds. V. Mannings, A. Boss & S.S. Russell (Tucson: University of Arizona press), in press

Davis, C.J., Matthews, H.E., Ray, T.P., Dent, W.R.F., Richer, J.S. 1999, MNRAS, 309, 141

Eiroa, C., & Casali, M.M. 1992, A&A, 262, 468

Eiroa, C., Palacios, J., Eislöffel, J., Casali, M.M., Curiel, S. 1997, in poster proceedings of IAU Symp. No. 182, F. Malbet & A. Castets eds., p. 103

Elmegreen, B.G. 1997, ApJ, 486, 944

Elmegreen, B.G. 1999, ApJ, 515, 323

Giovannetti, P., Caux, E., Nadeau, D., Monin, J.-L. 1998, A&A, 330, 990

Herbst, T.M., Beckwith, S.V.W., & Robberto, M. 1997, ApJ, 486, L59

Hodapp, K.W. 1999, AJ, 118, 1338

Hogerheijde, M.R., van Dishoeck, E.F., Salverda, J.M., Blake, G.A. 1999, ApJ, 513, 350

Hurt, R. L., & Barsony, M. 1993, ApJ, 460, L45

Kaas, A.A. 1999, AJ, 118, 558

Kroupa, P., Petr, M.G., McCaughrean, M.J. 1999, New Ast., 4, 495

de Lara, E., Chavarria–K., C., & López–Molina, G. 1991, A&A, 243, 139

McMullin, J. P., Mundy, L. G., Wilking, B. A., Hezel, T., & Blake, G. A. 1994, ApJ, 424, 222

Meyer, M.R., Adams, F.C., Hillenbrand, L.A., Carpenter, J.M., & Larson, R.B. 2000, in Protostars and Planets IV, eds. V. Mannings, A.P. Boss & S.S. Russell (Tucson: Univ. of Arizona Press), in press

Motte, F., André, P., & Neri, R. 1998, A&A, 336, 150

Myers, P.C. 1998, ApJ, 496, L109

Palla, F., & Stahler, S. 1999, ApJ, 525, 772

Rodríguez, L.F., Curiel, S., Moran, J.M., Mirabel, I.F., Roth, M., & Garay, G. 1989, ApJ, 346, L85

Salpeter, E.E. 1955, ApJ, 121, 161

Scalo, J.M. 1986, Fund. Cosm. Ph., 11, 1

Stahler, S.W., Palla, F. & Ho, P.T.P. 2000, in Protostars and Planets IV eds. V. Mannings, A.P. Boss & S.S. Russell (Tucson: Univ. of Arizona Press), in press

Strom, S.E., Vrba, F.J., & Strom, K.M. 1976, AJ, 81, 638

Testi, L., Palla, F., & Natta, A. 1999, A&A, 342, 515

Testi, L., & Sargent, A.I. 1998, ApJ, 508, L91 (TS98)

Testi, L., & Sargent, A.I. 2000, in Imaging at Radio through Submillimeter Wavelengths, eds. J. Mangum & S. Radford, ASP Conf. Series, in press

White, G.J., Casali, M.M., & Eiroa, C. 1995, A&A, 298, 594

Williams, J.P., & Myers, P.C. 1999, ApJ, 518, L37

Wolf-Chase, G.A., Barsony, M., Wootten, H.A., Ward-Thompson, D., Lowrance, P.J., Kastner, J.H., McMullin, J.P. 1998, ApJ, 501, L193

Table 1. N_2H^+(1–0) Cores Parameters

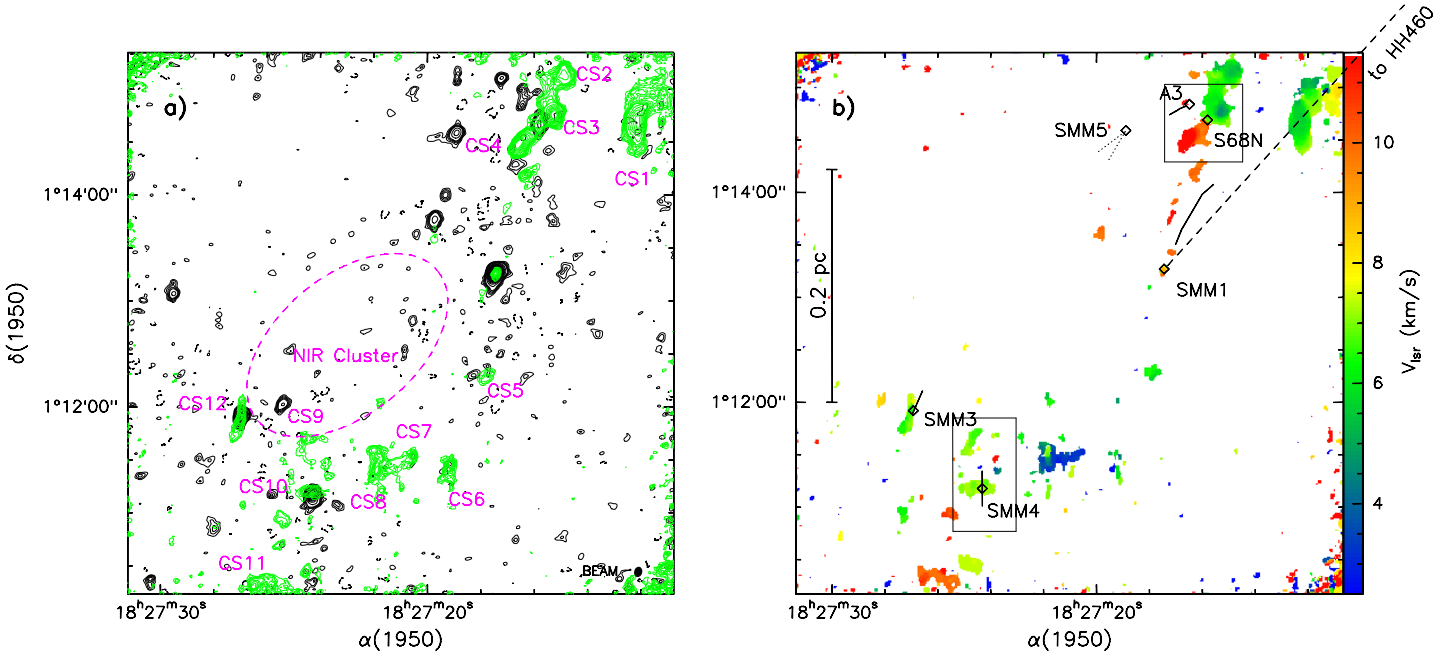| Name	$\Delta\alpha$ (1950)	$\Delta\delta$ (1950)	V_{LSR} (km/s)	ΔV (km/s)	M_{vir} ($M_\odot$)	f_{OVRO}	M_d ($M_\odot$)	$M_\star$ ($M_\odot$)
A	133	-177	7.15	0.7	–	–	–	–
B	88	-44	7.68	1.2	30	~20%	12	7
C	-44	44	8.35	1.1	18	–	14	2
D	-44	133	8.49	0.8	9	≤5%	5.5	2
Spur	–	–	8.32	0.7	–	–	–	–

Fig. 1.— a) Integrated intensity contours for CS(2–1) emission in the Serpens core are shown in green, overlaid on the 3 mm continuum map (TS98). Contour levels begin at 0.9 Jy km/s/beam (3σ) and are spaced by 0.3 Jy km/s/beam to 3 Jy km/s/beam and thereafter by 1 Jy km/s/beam. The dashed ellipse represents the NIR cluster (Kaas 1999). The CS features discussed in the text are marked CS1 to CS12. b) Color-coded map of the mean velocity variations across the CS structures of Fig. 1a. Known outflow sources, represented by open diamonds, are labelled and solid lines indicate the orientations of observed jets or, for SMM5, reflection nebulosity. The dashed line from SMM1 indicates the direction to HH460. The two rectangles mark the areas shown in Figure 2. Increased noise in the upper left and lower right corners of both images is due to loss of sensitivity at the edge of the mosaic.
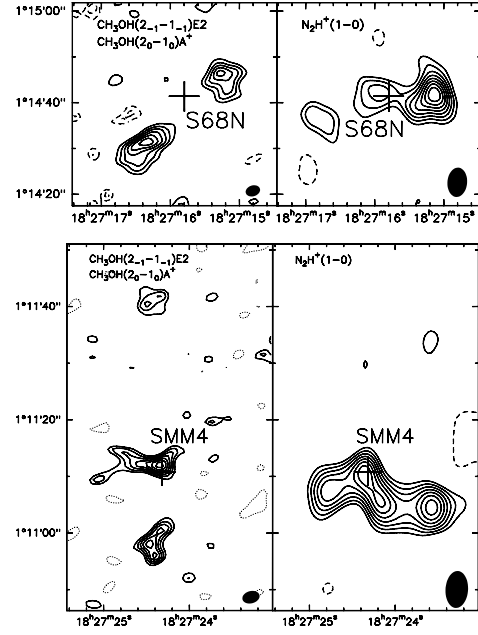
Fig. 2.— Integrated intensity maps of $CH_3OH(2_k–1_k)$ and $N_2H^+(1–0)$ for S68N and SMM4 the two regions indicated in Figure 1b. Synthesised beams (FWHM) are shown by black ellipses in the lower right corners. Contour levels start at 3σ and are spaced by 1σ (0.3 Jy km/s/beam for S68N and 0.2 Jy km/s/beam for SMM4).
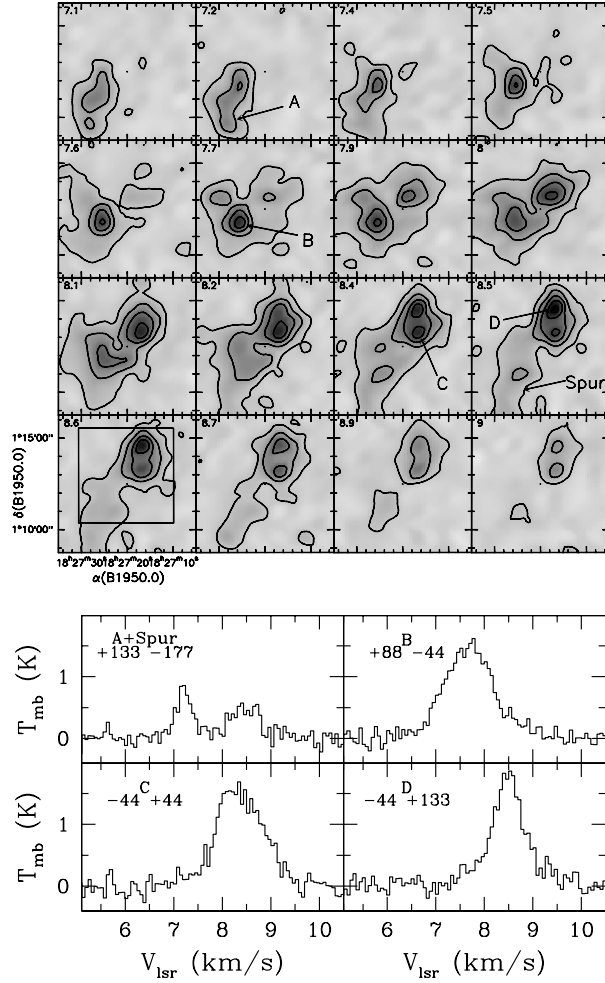
Fig. 3.— Top panel: FCRAO/SEQUOIA $N_2H^+(1_{01}$–$0_{12})$ channel maps. The five main kinematical structures, A, B, C, D, and the "Spur" are each labelled at their approximate V_{LSR}, which is given in the top-left corner of each panel. Contour levels are: 0.18 to 2.18 by 0.36 K. The square in the bottom left channel shows the area mapped at OVRO. Bottom panel: $N_2H^+(1_{01}$–$0_{12})$ spectra observed towards the four cores A, B, C, and D, as defined in Fig. 3. In each panel the offset in arcsec from position $\alpha = 18^h27^m20^s$, $\delta = 1°12'30''$ (B1950.0) is given.